Spin-Fluctuation Induced Anomalous Hall Effect in Distorted Kagome Antiferromagnet DyAgGe

Tomomi Furuhashi,[1] Keita Nagasawa,[2,3] Yuichi Yamasaki,[4,5] Hironori Nakao,[6]
Yusuke Kozuka,[7] Yoshihiro Tsujimoto,[7] Kazunari Yamaura,[7] and Jun Fujioka[8,9]

[1]*Graduate School of Science and Technology, University of Tsukuba, Tsukuba, Ibaraki 305-8573, Japan*

[2]*College of Engineering Sciences, University of Tsukuba, Tsukuba, Ibaraki 305-8573, Japan*

[3]*Institute for Solid State Physics, The University of Tokyo, Kashiwanoha 5-1-5, Kashiwa 277-8581, Japan*

[4]*Center for Basic Research on Materials, National Institute for Materials Science (NIMS), Tsukuba 305-0047, Japan*

[5]*International Center for Synchrotron Radiation Innovation Smart, Tohoku University, Sendai 980-8577, Japan*

[6]*Institute of Materials Structure Science, High Energy Accelerator Research Organization, Tsukuba, Ibaraki 305-0801, Japan*

[7]*Research Center for Materials Nanoarchitechtonics (MANA), National Institute for Materials Science (NIMS), Namiki, Tsukuba 305-0044, Japan*

[8]*Department of Materials Science, University of Tsukuba, Tsukuba, Ibaraki 305-8573, Japan*

[9]*Research Center for Organic-Inorganic Quantum Spin Science and Technology (OIQSST), University of Tsukuba, Tsukuba, Ibaraki 305-8573, Japan*

(Dated: October 30, 2025)

Abstract

We have investigated the magnetic property and charge-transport property for the kagome frustrated antiferromagnet DyAgGe with the ZrNiAl-type crystal structure by measurements of magnetization, resistivity and resonant X-ray scattering. The magnetization curve shows the 1/9-, 1/3-, 5/9- and 7/9-plateaus of saturated magnetization under the magnetic field along the c-axis before entering the forced ferromagnetic phase at 7.3 T and 2 K. Magnetic superlattice X-ray reflections with the modulation vector (1/3, 1/3, 0), resonantly enhanced at the Dy L_3 edge, are observed in these plateau phases. All of these phases, except for the 1/9-plateau phase, evolve into the paramagnetic phase around 12-15 K with strong competition among them in the field range of 4-6 T. Furthermore, we found the large negative magnetoresistivity and anomalous Hall resistivity not proportional to magnetic field or magnetization near and above the magnetic transition temperature around 3-7 T. For comparison, we also investigated the charge-transport for the isostructural magnet DyPtIn, which does not exhibit the field-induced multiple phase transitions. In contrast with the behavior of DyAgGe, DyPtIn does not show remarkable magnetoresistivity and anomalous Hall resistivity near and above the magnetic transition temperature. The anomalous Hall effect persisting above the magnetic transition temperature is likely caused by spin fluctuations enhanced by the competing multiple magnetic phases through the scalar spin chirality mechanism in DyAgGe.

I. INTRODUCTION

Electromagnetic response arising from nontrivial spin textures in magnetic metals has received of great interest in modern condensed matter physics. The anomalous Hall effect (AHE) or topological Hall effect (THE) is a typical example, where the Hall effect is induced by the magnetism in metals and semiconductors [1]. This is well exemplified by skyrmion magnets, which typically emerge in chiral and geometrically frustrated magnetic systems [2, 3]. In skyrmion magnets, itinerant electrons moving on noncoplanar spin texture acquire the spin Berry phase proportional to the scalar spin chirality (SSC), which is defined by the solid angle subtended by three spins as $\chi = S_1 \cdot (S_2 \times S_3)$ [4–9]. The spin Berry phase acts as the fictitious magnetic field for itinerant electrons, thereby giving rise to the topological Hall effect. In particular, the SSC is scaled to the Skyrmion density in real space and/or momentum space, and its modulation often results in the giant THE, offering potential for spintronic applications.

In addition to the case of long-range ordered noncoplanar spin textures, the Hall effect can also arise from fluctuating or spatially inhomogeneous spin textures that lack long-range magnetic ordering. Conventionally, it is known that electron scattering off localized magnetic defects can give rise to the extrinsic AHE via skew scattering or side-jump mechanisms [1]. The extrinsic AHE is generally small in its magnitude, but recent studies demonstrate that it can be remarkably enhanced by spin fluctuation or magnetic domain walls in topological semimetals [10, 11]. On the other hand, it has been also known that the transient noncoplanar spin textures generated by thermal spin fluctuations can induce AHE through the SSC. Indeed, in double-exchange ferromagnets, the AHE emerging near the transition temperature has been attributed to thermally induced topological spin texture [12, 13]. More recently, it has been demonstrated that spin fluctuations can trigger the large AHE with the tangent of anomalous Hall angle ($\tan \theta_{\mathrm{H}}$) more than 0.01 [14–20]. Notably, the large AHE due to the thermally induced SSC has been observed even in collinear antiferromagnets. For example, a recent study argues that thermally induced solitonic spin fluctuations can cause large AHE that persists far above the magnetic transition temperature in collinear antiferromagnets exhibiting a magnetic devil's staircase [18]. Nevertheless, it remains unclear what kind of magnetic ordering or phase transition induces the large AHE persisting above the transition temperature, and thus its observation has been limited to a few magnetic metals.

In this context, geometrically frustrated magnets with unconventional spin excitation or magnetic transition offer a platform to search the remarkable spin-fluctuation induced AHE. The RAgGe (R =Tb-Lu) is one of typical frustrated magnetic metals, which crystallize in the ZrNiAl-type structure [21]. As shown in Figs. 1(a) and (b), the R-site forms the distorted kagome lattice in the ab-plane, which stacks along the c-axis. The magnetic interaction of R-4f moment is mediated by conduction electrons, and the competing intersite interaction or geometrically frustrated interaction induce a variety of unconventional magnetic states for R=Tb, Dy and Ho [21–23]. For example, HoAgGe exhibits several magnetic phases with noncollinear magnetic structure including the spin ice state under the magnetic field along the b-axis [23–25]. In particular, the recent studies demonstrate that the AHE persists in wide temperature regime up to about four times of the magnetic transition temperature, which is attributed to the skew scattering from fluctuating spins [26].

Field-induced multiple phase transitions are also observed in DyAgGe, which exhibits collinear antiferromagnetic orderings. In this material, the antiferromagnetic ordering occurs at 15 K (= $T_{\rm N1}$), followed by a second magnetic transition at 12 K (= $T_{\rm N2}$) under zero magnetic field [22, 23]. The wave vector of the antiferromagnetic ordering is characterized by $(1/3, 1/3, 0)$, and the Dy magnetic moment lies in the bc-plane, forming a tilt angle of about 50° with respect to the c-axis, as shown in Figs. 1(a) and (b). Such multiple magnetic phase transitions on the kagome lattice may induce peculiar spin fluctuations and magneto-transport properties in DyAgGe, but these phenomena have not been elucidated so far. In this study, we investigated the magnetic property and magneto-transport property for DyAgGe by measurements of magnetization, Hall resistivity and the resonant magnetic X-ray scattering.

II. EXPERIMENTAL METHODS

Single crystalline samples of DyAgGe were grown by using the Ag-Ge rich self-flux technique [23]. The starting materials Dy, Ag, and Ge were placed in an aluminum crucible in a molar ratio of 1 : 6.8 : 2.3, and sealed in an evacuated quartz ampoule. The quartz ampoule was heated up to 1100 °C, held at that temperature for 24 h, and then cooled to 850 °C over 135 h. Following slow cooling, the ampoule was quenched to room temperature, and the remaining solution was separated by centrifugation. The single crystal

was ground into powder form, which was examined by X-ray diffraction using a commercial diffractometer (Rigaku MiniFlex) with Cu-Kα_1 and -Kα_2 radiation sources [see also Fig. S1] [27]. Resistivity measurements were performed using the four-probe method in a Physical Property Measurement System (Quantum Design) over the temperature range of 2–300 K and in magnetic field up to 14 T. The magnetization measurements were performed using the Dynacool System equipped with the VSM option from 2 K to 300 K under the magnetic field up to 14 T. The resonant magnetic X-ray scattering was performed under the magnetic field at the BL-3A, Photon Factory of KEK, Japan. The magnetic field was applied along the c-axis up to 6 T by using a commercial superconducting magnet.

III. RESULTS AND DISCUSSION

Figure 1(c) shows the temperature dependence of magnetization for DyAgGe under the magnetic field (B) along the c-axis. For $B = 0.1$ T and 0.5 T, the magnetization shows two anomalies at $T_{\rm N1}$ and $T_{\rm N2}$, consistent with previous studies [22, 23]. Above 2 T, the anomaly at $T_{\rm N1}$ remains, whereas that at $T_{\rm N2}$ is not clearly observed except for the case of $B = 5$ T. Figure 1(d) shows the field dependence of magnetization at various temperatures. At 2 K, the magnetization exhibits plateaus at 1/9, 1/3, 5/9 and 7/9 of the saturated magnetization [see also the inset to Fig. 1(d)] and is nearly constant above 7.6 T. Here, the 5/9-plateau phase is clearly visible only during the process of increasing the magnetic field [see inset to Fig. 1(d)]. All data shown below under finite magnetic fields were measured during the process of increasing the magnetic field. We note that the saturated magnetization is about 6.4 μ_B/f.u., which is consistent with the expected value for the Dy-4f moment (9.9 μ_B) tilted by approximately 50° from the c-axis. With increasing temperatures, these plateaus are gradually smeared out and vanish around 14 K.

Based on the magnetization results, we constructed the magnetic phase diagram in the temperature–field plane as shown in Fig. 2 (a). The 1/9-plateau phase is confined to the low-field, low-temperature region below approximately 1.3 T and $T_{\rm N2}$, while the 1/3-plateau phase (7/9-plateau phase) extends over a relatively wide field–temperature region of 1–4.5 T (5.4–7.1 T). Notably, the 5/9-plateau phase emerges within a narrow region between the 1/3- and 7/9-plateau phases. According to the previous study, at 1.5 K, the Dy-4f moments show the collinear antiferromagnetic structure with a wave vector of (1/3, 1/3, 0),

forming the $\sqrt{3} \times \sqrt{3}$ magnetic unit cell at zero magnetic field [22]. To gain insight into the magnetic state under the magnetic field, we investigated the magnetic wave vector by means of resonant X-ray scattering.

Figure 2(b) shows the scattering spectrum of $(H, 8/3, 0)$ magnetic superlattice reflection measured at 4.5 K [see also Fig. S2] [27]. The incident X-ray is nearly π-polarized, but the scattered X-ray includes both σ'- and π'-polarized components. Here, σ and π denote the polarization component perpendicular and parallel to the scattering plane, respectively. At 0 T, a clear peak is observed around $H = 0.67$, which is consistent with the antiferromagnetic structure with the wave vector (1/3, 1/3, 0). The peak becomes more pronounced at 2 T but diminishes above 4.8 T. We plot the integrated intensity and full width at half maximum of peak as a function of magnetic field in Fig. 2(c). With increasing the magnetic field, the peak intensity slightly increases in the 1/3-plateau phase, decreases sharply near B_{c2} (= 4.7 T) and becomes nearly constant above 5 T. This is in contrast with the behavior of peak width, which does not significantly change under the magnetic field. These results suggest that the antiferromagnetic structures with $\sqrt{3} \times \sqrt{3}$ magnetic unit cell is maintained in the 1/3-, 5/9-, and 7/9-plateau phases, while the detail of magnetic structure could not be determined at the present stage [see also Fig. S3] [27].

With the magnetic phase diagram established, we proceed to discuss the charge transport properties. Figure 3(a) shows the temperature dependence of resistivity (ρ_{xx}). At 0 T, the resistivity shows a sharp peak at T_{N1}, attributed to the carrier scattering by spin fluctuation, while only a slight change in gradient is observed at T_{N2}. Figure 4(a) shows the magnetoresistivity measured for $B||c$ at various temperatures. At 2 K, four anomalies due to the field-induced phase transition are clearly observed in agreement with the results of magnetization. With increasing temperature, the anomalies gradually diminish, and only a single peak remains at 14 K. Above 16 K, the peak structure is no longer observed, but the magnetoresistivity exhibits a downturn around 3-7 T. The negative magnetoresistivity is most pronounced near T_{N1}, but remains observable even at high temperatures. To quantify the temperature dependence of negative magnetoresistivity, we plotted the magnetoresistivity-ratio defined as $\Delta\rho_{xx}/\rho_{xx}(0\ \mathrm{T})$ with $\Delta\rho_{xx} = [\rho_{xx}(14\ \mathrm{T}) - \rho_{xx}(0\ \mathrm{T})]$ in Fig. 3(b). The significant negative magnetoresistivity is observed not only near T_{N1} but also up to around 60 K. This suggests that the spin fluctuation occurs over wide temperature range above T_{N1}, resulting in the remarkable electrons scattering.

Figure 4(b) shows the Hall resistivity (ρ_{yx}) at various temperatures. At 2 K, ρ_{yx} increases almost linearly with the magnetic field up to 5 T and above 7.6 T, primarily due to the ordinary Hall effect, and displays several anomalies due to the magnetic transitions in intermediate field region. As the temperature increases, the anomalies gradually diminish and evolve into a hump-like structure around 6 T at 12 K. Interestingly, the remnant of the hump-like structure persists even above $T_{\rm N1}$, leading to a B-nonlinear behavior of ρ_{yx} up to around 40 K. Finally, the B-linear dependence is recovered at around 100 K.

In general, the Hall effect in magnetic metals originates from the anomalous or topological Hall effect in addition to the ordinary Hall effect. To qualitatively evaluate each contribution, we derived the Hall conductivity $\sigma_{xy} = \rho_{yx}/(\rho_{xx}^2 + \rho_{yx}^2)$, and analyzed it using the following three-component-model,

$$\sigma_{xy} = \sigma_{xy}^{O} + \sigma_{xy}^{M} + \sigma_{xy}^{notM} \tag{1}$$

The first, second and third terms represent the ordinary Hall component [$\sigma_{xy}^{O} = R_{\rm O}B/(\rho_{xx}^2 + \rho_{yx}^2)$], the anomalous Hall component in proportion to M ($\sigma_{xy}^{M} = S_A M$) and the residual component (σ_{xy}^{notM}), which is proportional neither to B nor to M, respectively. Here, we assumed the intrinsic mechanism in the coherent transport regime for σ_{xy}^{M} [1, 28]. Figure 5 displays the analyzed results as well as the magnetization curve. At 2 K, σ_{xy} shows several steps or dips at field-induced magnetic transitions. Except these anomalies, σ_{xy} is well reproduced by the sum of σ_{xy}^{O} and σ_{xy}^{M} ($\sigma_{xy}^{O} + \sigma_{xy}^{M}$) as exemplified in Fig. 5(a2). Consequently, σ_{xy}^{notM} is vanishingly small over the entire magnetic field range [see Fig. 5(a3)]. At 14 K, $\sigma_{xy}^{O} + \sigma_{xy}^{M}$ is slightly deviated from σ_{xy} around 6 T, resulting in a peak structure of σ_{xy}^{notM}. The deviation is much enhanced at 30 K, and consequently, σ_{xy}^{notM} exhibits a pronounced peak around 8 T. At 50 K, a similar behavior is observed, but σ_{xy}^{notM} appears to be slightly suppressed. At 100 K, σ_{xy} is again well reproduced by $\sigma_{xy}^{O} + \sigma_{xy}^{M}$, resulting in the negligible σ_{xy}^{notM}.

To visualize the field-temperature variation of σ_{xy}^{notM}, we show the contour plot of σ_{xy}^{notM} on the temperature-field plane in Fig. 6(a). σ_{xy}^{notM} is small in the magnetically ordered phases but is remarkably enhanced near and above $T_{\rm N1}$ around 4-10 T, below which the 1/3-, 5/9-, 7/9-plateaus and enforced ferromagnetic phases are keenly competing with each other. We also show the temperature dependence of σ_{xy}^{M} and σ_{xy}^{notM} at 8.5 T in Fig. 3(c).

σ_{xy}^{notM} is typically less than 50 Ω^{-1}cm^{-1} below $T_{\rm N1}$, but remarkably increases above $T_{\rm N1}$, reaching about 150 Ω^{-1}cm^{-1} around 30 K. At higher temperatures, it gradually decreases and becomes substantially small at 80 K. On the other hand, σ_{xy}^{M} is nearly temperature independent below $T_{\rm N2}$ but is discontinuously enhanced at $T_{\rm N2}$. In particular, the tangent of anomalous Hall angle (tan $\theta_{\rm AH}$) reaches more than 0.02 at 12 K. With increasing temperature, σ_{xy}^{M} monotonically decreases but remains to be substantial at 80 K. We note that σ_{xy}^{notM} reaches about one-half of σ_{xy}^{M} around 30 K, whereas the former is smaller than the latter in all temperature regions.

To clarify the relationship between the magnetic ordering and anomalous Hall response, it is instructive to compare with the results for DyPtIn, which also crystallizes in the ZrNiAl-type structure but exhibits ferromagnetic ordering with canted spin structure at 27 K [29, 30]. Figures 7 (a)-(d) show the resistivity, magnetization, σ_{xy} and σ_{xy}^{notM}, respectively. As shown in Fig. 7(a), the resistivity shows a typical metallic behavior with a small anomaly around 22 K, which is slightly lower than the transition temperature in the previous report [see also the inset to Fig. 7(a)]. This is in contrast with the remarkable anomaly at $T_{\rm N1}$ for DyAgGe. As shown in Fig. 7(b), the magnetization curve shows a simple ferromagnetic-like behavior with the saturated magnetization about 6 μ_B/f.u.. This is consistent with the previous report, which demonstrates that the easy axis is tilted by about 37° from c-axis, similar to the case of DyAgGe [30]. As shown in Fig. 7(c), σ_{xy} shows a step-like structure below 1 T and nearly linearly increases with the magnetic field at 2 K. The former and latter are attributed to the anomalous Hall component and ordinary Hall component, respectively. As temperature increases, the step-like anomaly becomes progressively smeared out, leading to a broad dip around 4 T at 40 K. Notably, σ_{xy} is well fitted by $\sigma_{xy}^{O} + \sigma_{xy}^{M}$ over the entire temperature range, resulting in the small σ_{xy}^{notM}. These results suggest that the enhanced σ_{xy}^{notM} above $T_{\rm N1}$ in DyAgGe originates from the unconventional spin fluctuation associated with the multiple field-induced phase transitions, or equivalently, competing magnetic phases.

On the basis of these results, we consider the mechanism of AHE persisting above the magnetic transition temperature. At first, we consider the mechanisms of σ_{xy}^{M}. One possible mechanism is conventional skew scattering from spin fluctuation. However, it is recognized that the magnitude of skew scattering is not significant unless the charge transport is in the highly conductive regime $\rho_{xx} < 10^{-5}$ Ωcm. In the present material, the resistivity is more than about 5×10^{-4} Ωcm [see Fig. 3(a)]. Therefore, the relatively large tan $\theta_{\rm AH}$ (> 0.02) may

not be explained by the conventional skew scattering mechanism. More plausible scenario is the intrinsic mechanism (Berry curvature mechanism) in momentum space. Indeed, recent study argues that the Weyl nodes emerge near the Fermi energy in HoAgGe [26]. The significant Berry curvature due to Weyl nodes may also induced σ_{xy}^{M} with relatively large anomalous Hall angle in the present material.

On the other hand, σ_{xy}^{notM} gradually increases above $T_{\rm N1}$ and reaches the maximum around 30 K, indicating that its origin is different from that of σ_{xy}^{M}. The enhancement of σ_{xy}^{notM} above magnetic transition temperature is unconventional, but recent studies suggest that the SSC induced by thermal spin fluctuation can cause the anomalous Hall effect or topological Hall effect even above the magnetic transition temperature [16, 17, 19, 31, 32]. It is well known that the sum of the thermally induced SSC among three neighbouring sites on the kagome lattice over the entire crystal is finite, which manifests as the finite Hall signal [5–7]. In Fig. 6 (b), we plot σ_{xy}^{notM} as a function of the magnetization normalized by the saturation magnetization (M/M_s), where M_s is defined as the magnetization at 2 K and 14 T. Near and above $T_{\rm N1}$, σ_{xy}^{notM} at various temperatures commonly exhibits a maximum around $M/M_s = 0.6-0.8$, indicating that σ_{xy}^{notM} is enhanced in partially spin polarized state. Similar AHE or THE are often observed in ferromagnets or frustrated magnets with complex spin texture, which are attributed to the SSC-induced Berry phase or multiple skew scattering [13, 17–19, 33–35]. In this context, it is likely that σ_{xy}^{notM} originates from the SSC-induced Berry phase or multiple skew scattering mechanism in the present material. Recent theoretical studies based on J_1-J_2-J_3 Ising model on the kagome lattice propose the emergence of classical spin liquid phase with 1/9-, 1/3-, 5/9- and 17/27-magnetization plateaus, which can be viewed as the self-organization of unconventional domain-wall structure or spin clusters [36, 37]. Although the magnetic structure of each plateau phase is not clear in DyAgGe, the fluctuation of similar domain-wall structure or cluster spin excitation promoted by the multiple phase competition may cause the SSC and resultant AHE persisting in the wide temperature-field region.

IV. CONCLUSION

In this study, we have investigated the magnetic property and charge-transport for the kagome antiferromagnet DyAgGe, which crystallizes in the ZrNiAl-type structure, with a

focus on the anomalous Hall effect due to the spin fluctuation. The magnetization curve shows the 1/9-, 1/3-, 5/9- and 7/9-plateau under the magnetic field before reaching the forced ferromagnetic phase at 2 K. The 1/9-plateau (5/9-plateau) phase is observed in narrow region below 1 T (around 5 T), below 10-11 K, respectively. On the contrary, the 1/3- and 7/9-plateau phases appear over relatively wide field ranges and turn into the paramagnetic state around 13-15 K. The results of resonant magnetic X-ray scattering show that the magnetic superlattice reflection with the wave vector (1/3, 1/3, 0) commonly appears in these plateau phases, indicating the antiferromagnetic or ferrimagnetic ordering with the $\sqrt{3} \times \sqrt{3}$ unit cell. The negative magnetoresistivity becomes remarkable around 3-7 T and 15 K, below which the 1/3-, 5/9- and 7/9-plateau phases are strongly competing with each other. Moreover, the anomalous Hall conductivity not proportional to magnetic field or magnetization grows up above 15 K with increasing temperature. In particular, the anomalous Hall conductivity exhibits a maximum around 30 K and persists up to approximately 60 K. As a comparison, we also examined the magnetic property and magneto-transport property for the isostructural DyPtIn without complex magnetic transitions. In this material, the pronounced anomalous Hall resistivity not proportional to the magnetic field or magnetization is not observed both below and above the magnetic transition temperature. Based on the analysis of Hall conductivity, it is likely that the thermal spin fluctuation, enhanced by the competing multiple magnetic phases, gives rise to the scalar-spin-chirality-related anomalous Hall effect persisting well above the magnetic transition temperature.

ACKNOWLEDGEMENTS

This work was partly supported by Grant-In-Aid for Science Research (Nos. 21K18813, 22H01177, 24K03205, 24H01685, 25K01657) from the MEXT, by Iketani Foundation for Materials Science and Engineering, Japan, by JST FOREST Program (Grant Number: JPMJFR203D), and by JST-CREST (Grant Number: JPMJCR2435). MANA is supported by World Premier International Research Center Initiative (WPI), MEXT, Japan. The synchrotron powder XRD was performed with the approvals of the Photon Factory Program

Advisory Committee (Proposals No. 2021S2-004).

[1] N. Nagaosa, J. Sinova, S. Onoda, A. H. MacDonald, and N. P. Ong, Rev. Mod. Phys. **82**, 1539 (2010).

[2] A. Neubauer, C. Pfleiderer, B. Binz, A. Rosch, R. Ritz, P. G. Niklowitz, and P. Boni, Phys. Rev. Lett. **102**, 18602 (2009).

[3] M. Lee, W. Kang, Y. Onose, Y. Tokura, and N. P. Ong, Phys. Rev. Lett. **102**, 186601 (2009).

[4] J. Ye, Y. B. Kim, A. J. Millis, B. I. Shraiman, P. Majumdar, and Z. Tesanovic, Phys. Rev. Lett. **83**, 3737 (1999).

[5] K. Ohgushi, S. Murakami, and N. Nagaosa, Phys. Rev. B **62**, R6065 (2000).

[6] Y. Taguchi, Y. Oohara, H. Yoshizawa, N. Nagaosa, and Y. Tokura, Science **291**, 2573 (2001).

[7] G. Tatara and H. Kawamura, J. Phys. Soc. Jpn **71**, 2613 (2002).

[8] M. Onoda, G. Tatara, and N. Nagaosa, J. Phys. Soc. Jpn. **73**, 2624 (2004).

[9] P. Bruno, V. K. Dugaev, , and M. Taillefumier, Phys. Rev. Lett. **93**, 096806 (2004).

[10] W. Xia, B. Bai, X. Chen, Y. Yang, Y. Zhang, J. Yuan, Q. Li, K. Yang, X. Liu, Y. Shi, *et al.*, Phys. Rev. Lett. **133**, 216602 (2024).

[11] O. K. Forslund, X. Liu, S. Shin, C. Lin, M. Horio, Q. Wang, K. Kramer, S. Mukherjee, T. Kim, C. Cacho, *et al.*, Phys. Rev. Lett. **134**, 126602 (2025).

[12] P. Matl, N. P. Ong, Y. F. Yan, Y. Q. Li, D. Studebaker, T. Baum, , and G. Doubinina, Phys. Rev. B **57**, 10248 (1998).

[13] S. H. Chun, M. B. Salamon, Y. Lyanda-Geller, P. M. Goldbart, and P. D. Han, Phys. Rev. Lett. **84**, 757 (2000).

[14] H. Ishizuka and N. Nagaosa, Sci. Adv. **4**, eaap9962 (2018).

[15] Y. Fujishiro, N. Kanazawa, R. Kurihara, H. Ishizuka, T. Hori, F. S.Yasin, X. Yu, A. Tsukazaki, M. Ichikawa, M. Kawasaki, *et al.*, Nat. Commun. **12**, 317 (2021).

[16] M. Uchida, S. Sato, H. Ishizuka, R. Kurihara, T. Nakajima, Y. Nakazawa, M. Ohno, M. Kriener, A. Miyake, K. Ohishi, *et al.*, Sci. Adv. **7**, eabl5381 (2021).

[17] K. K, Kolincio, M. Hirschberger, J. Masell, T. hisa Arima, N. Nagaosa, , and Y. Tokura, Phys. Rev. Lett. **130**, 136701 (2021).

[18] N. Abe, Y. Hano, H. Ishizuka, Y. Kozuka, T. Tadano, Y. Tsujimoto, K. Yamaura, S. Ishiwata, and J. Fujioka, npj Quantum Mater. **9**, 41 (2024).

[19] H. Jeon, H. Seo, J. Seo, Y. Kim, E. S. Choi, Y. Jo, H. N. Lee, J. M. Ok, and J. S. Kim, Commun. Phys. **7**, 162 (2024).

[20] K. Karube, Y. Onuki, T. Nakajima, H.-Y. Chen, H. Ishizuka, M. Kimata, T. Ohhara, K. Munakata, T. Nomoto, R. Arita, T. hisa Arima, Y. Tokura, and Y. Taguchi, npj Quantum Mater. **10**, 55 (2025).

[21] B. Gibson, R. Pottgen, R. K. Kremer, A. Simon, and K. R. Ziebeck, Journal of Alloys and Compounds **239**, 34 (1996).

[22] S. Baran, M. Hofmann, J. Leciejewicz, B. Penc, M. Slaski, and A. Szytula, Journal of Alloys and Compounds **281**, 92 (1998).

[23] E. Morosan, S. Budko, P. Canfield, M. S. Torikachvilic, and A. Lacerda, J. Magn. and Magn. Mater. **277**, 298 (2004).

[24] K. Zhao, H. Deng, H. Chen, K. A. Ross, V. Petricek, G. Gunther, M. Russina, V. Hutanu, and P. Gegenwart, Science **367**, 1218 (2020).

[25] H. Bhandari, P.-H. Chang, R. B. Regmi, B. G. Markus, L. Forro, J. F. Mitchell, I. I.Mazin, and N. J. Ghimire, Commun. Mater. **6**, 52 (2025).

[26] S. Roychowdhury, K. Samanta, S. Singh, W. Schnelle, Y. Zhang, J. Noky, M. Vergniory, C. Shekhar, , and C. Felser, Proc. Natl. Acad. Sci. U.S.A. **121**, e2401970121 (2024).

[27] See Supplemental Material for the sample characterization and resonant magnetic X-ray diffraction.

[28] S. Onoda, N. Sugimoto, and N. Nagaosa, Phys. Rev. Lett. **97**, 126602 (2006).

[29] E. Morosan, S. L. Bud'ko, and P. C. Canfield, Phys. Rev. B **72**, 014425 (2005).

[30] S. Baran, L. Gondek, J. Hernandez-Velasco, D. Kaczorowski, and A. Szytula, J. Magn. Magn. Mater. **305**, 196 (2006).

[31] K. S. Denisov, I. V. Rozhansky, N. S. Averkiev, and E. Lahderanta, Phys. Rev. B **98**, 195439 (2018).

[32] H. Ishizuka and N. Nagaosa, Phys. Rev. B **103**, 235148 (2021).

[33] N. J. Ghimire, R. L. Dally, L. Poudel, D. Jones, D. Michel, N. T. Magar, M. Bleuel, M. A. McGuire, J. Jiang, J. Mitchell, *et al.*, Sci. Adv. **6**, eabe2680 (2020).

[34] W. Yao, S. Liu, H. Kikuchi, H. Ishikawa, O. S. Fjellvag, D. W. Tam, F. Ye, D. L. Abernathy, G. D. A. Wood, D. Adroja, *et al.*, Phys. Rev. Lett. **134**, 186501 (2025).

[35] P. R. Baral, V. Ukleev, I. Zivkovic, Y. Lee, F. Orlandi, P. Manuel, Y. Skourski, L. Keller, A. Stunault, J. A. Rodriguez-Velamazan, *et al.*, Nature Commun. **16**, 3898 (2025).

[36] T. Mizoguchi, L. D. C. Jaubert, and M. Udagawa, Phys. Rev. Lett. **119**, 077207 (2017).

[37] K. Tokushuku, T. Mizoguchi, L. D. C. Jaubert, and M. Udagawa, J. Phys. Soc. Jpn **89**, 053408 (2020).

[38] K. Momma and F. Izumi, J. Appl. Cryst. **44**, 1272 (2011).

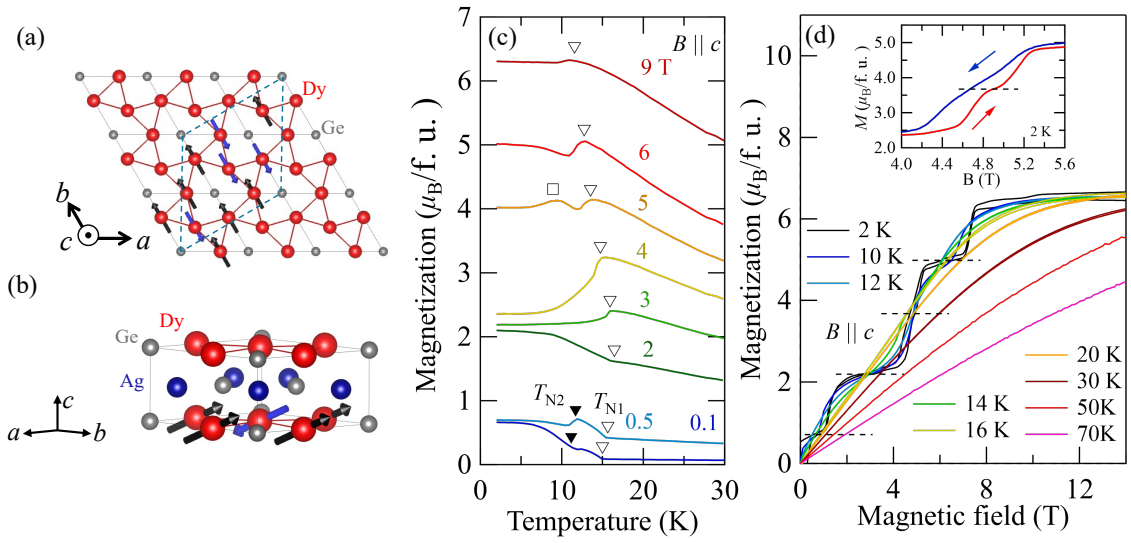

FIG. 1. (a) The schematic view of kagome layer of RAgGe with R = Dy [38]. The Dy constitutes the distorted kagome lattice in the ab-plane. Arrows denote the Dy-4f moment. Solid line and dashed line denote the unit cell and magnetic unit cell, respectively. (b) The crystal structure of DyAgGe. The Dy-4f moment is tilted by about 50° from c-axis in the bc-plane. (c) The temperature of magnetization of DyAgGe for $B||c$. Open and closed triangles denote $T_{\rm N1}$ and $T_{\rm N2}$, respectively. (d) The field dependence of magnetization of DyAgGe for $B||c$. The dashed line denotes the 1/9, 1/3, 5/9 and 7/9-plateau. The inset shows the magnified view of magnetization for 5/9-plateau.

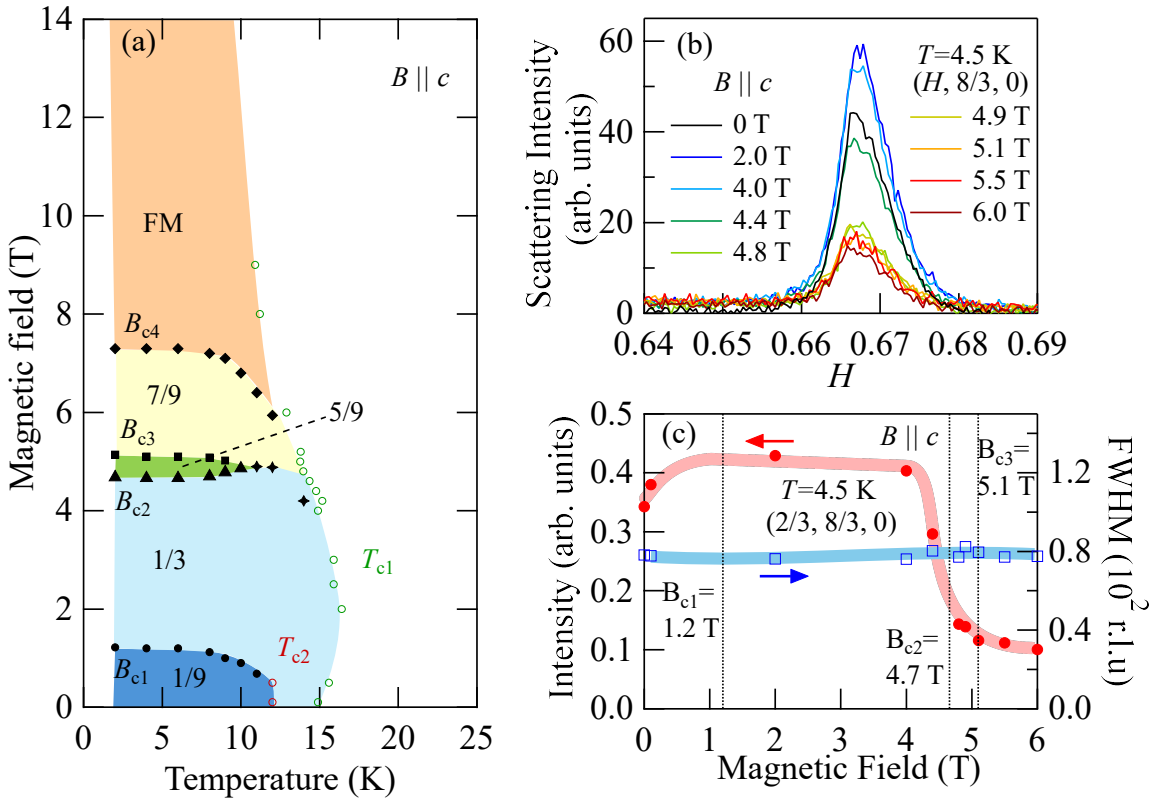

FIG. 2. (a) The magnetic phase diagram for DyAgGe. Closed (open) symbols are determined from the field (temperature) dependence of magnetization. (b) The resonant magnetic X-ray scattering around (H, 8/3, 0). The incident beam is π-polarized, while the scattered X-ray contains both σ'- and π'-polarization. (c) The closed circles and open squares denote the field dependence of scattering intensity and full width at half maximum (FWHM) of (2/3, 8/3, 0) reflection. The thick line is the guide to eyes.

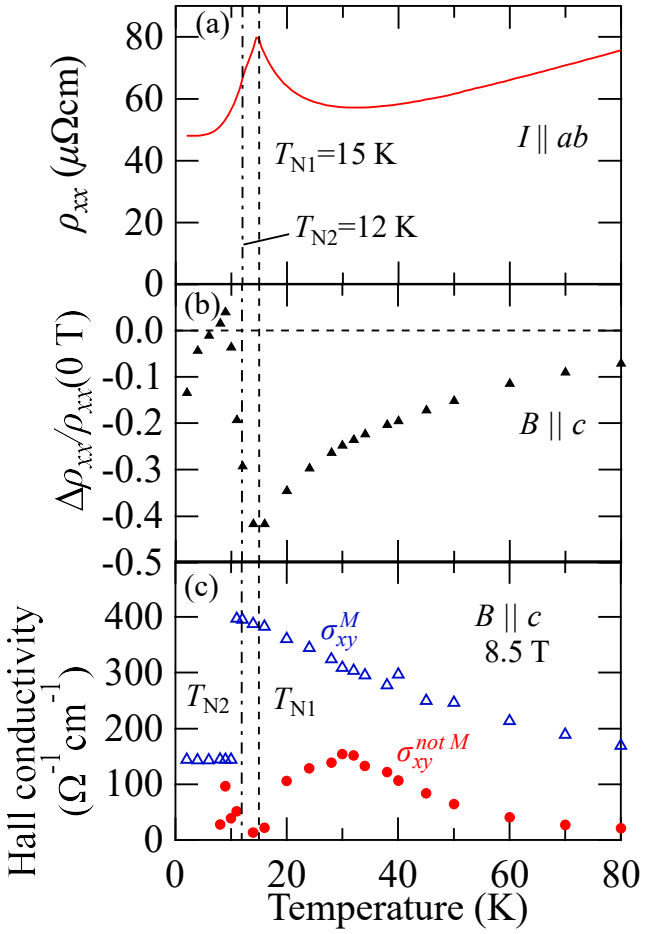

FIG. 3. (a) The temperature dependence of resistivity in the *ab*-plane under the zero magnetic field. (b) The temperature dependence of magnetoresistivity-ratio defined as $\Delta\rho_{xx}/\rho_{xx}(0\ \mathrm{T})$ with $\Delta\rho_{xx} = [\rho_{xx}(14\ \mathrm{T}) - \rho_{xx}(0\ \mathrm{T})]$. (c) The anomalous Hall conductivity in proportion to magnetization σ_{xy}^{M} (open triangles) and that not proportional to magnetic field and magnetization σ_{xy}^{notM} (closed circles) at 8.5 T.

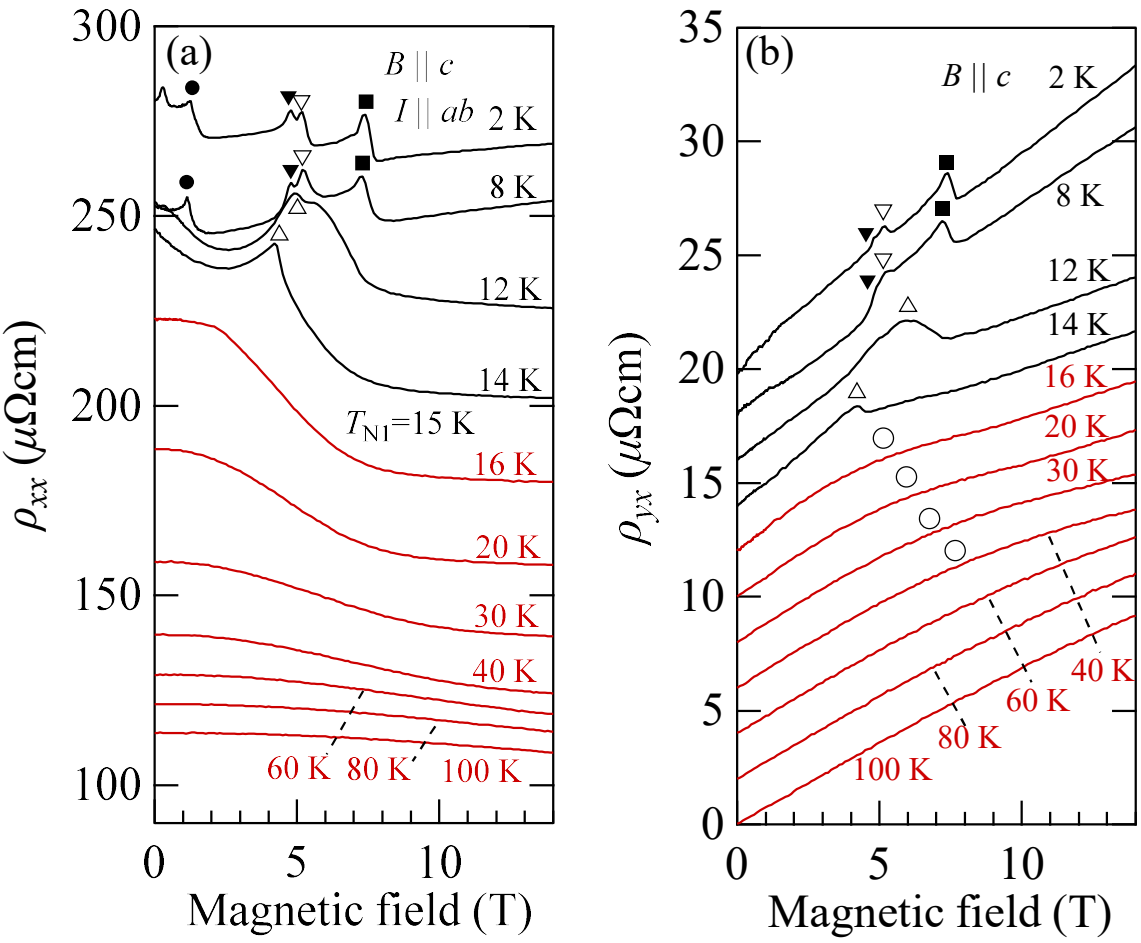

FIG. 4. (a) The magnetoresistivity (b) the Hall resistivity for DyAgGe. ρ_{xx} (ρ_{yx}) below 100 K is offset by 20$\mu\Omega$cm (2$\mu\Omega$cm) for clarity. The magnetoresistivity and Hall resistivity were measured as the magnetic field was increased. The closed circle, closed triangle, open triangle and closed square denote the magnetic transitions at B_{c1}, B_{c2}, B_{c3} and B_{c4}, respectively. The open circle in (b) shows the hump-like structure of ρ_{yx} (see also the main text).

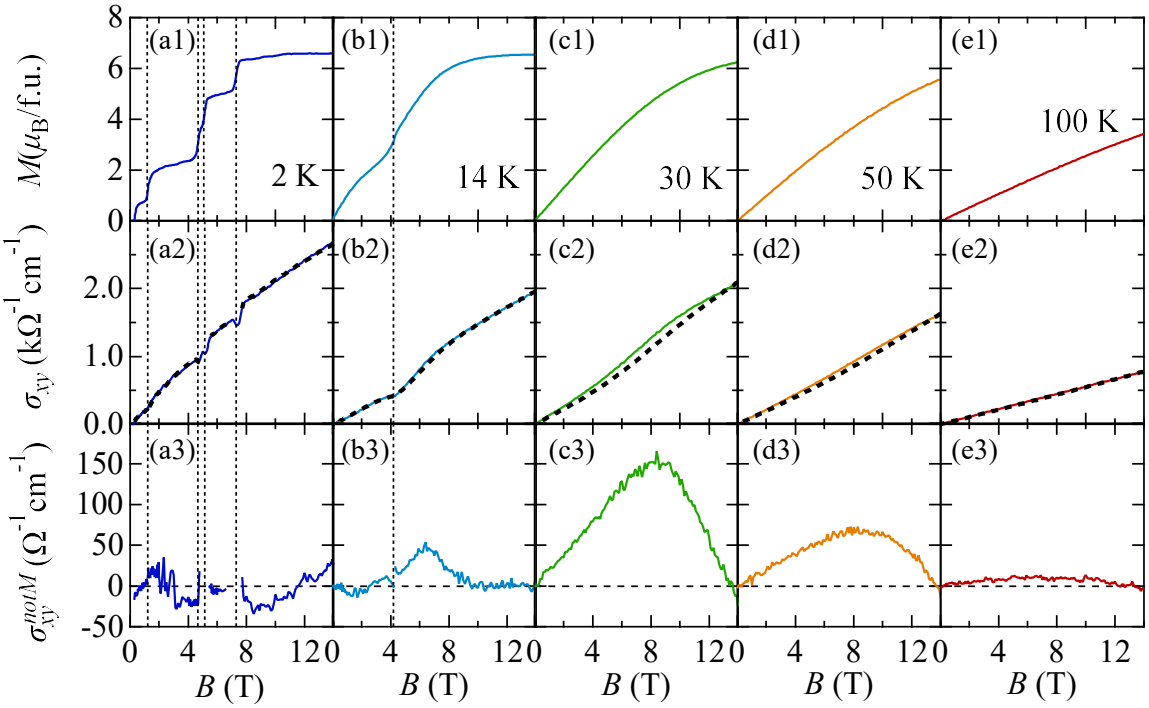

FIG. 5. The magnetization M, Hall conductivity σ_{xy} and Hall conductivity not proportional to the magnetic field and magnetization σ_{xy}^{notM} for DyAgGe. The dashed curves in (a2)-(e2) denote the sum of the ordinary Hall conductivity and anomalous Hall conductivity proportional to M ($\sigma_{xy}^{O} + \sigma_{xy}^{M}$). The vertical dashed lines denote the magnetic transitions at B_{c1}, B_{c2}, B_{c3} and B_{c4}.

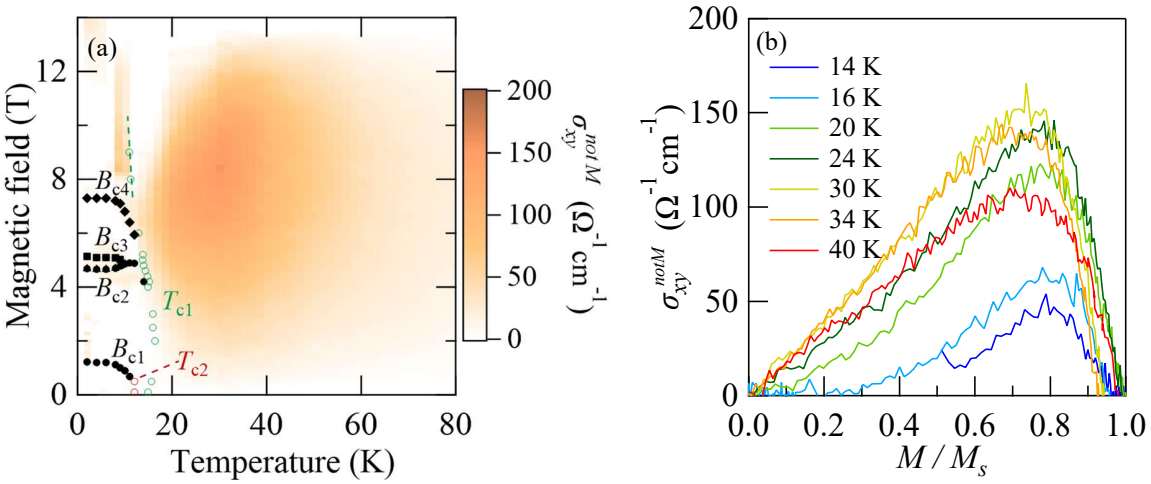

FIG. 6. (a) The contour plot of anomalous Hall conductivity not proportional to M (σ_{xy}^{notM}) for DyAgGe. The closed circle, closed triangle, open triangle and closed square denote the magnetic transitions at B_{c1}, B_{c2}, B_{c3} and B_{c4}, respectively. (b) σ_{xy}^{notM} as a function of normalized magnetization (M/M_s) with M_s being the magnetization at 2 K and 14 T.

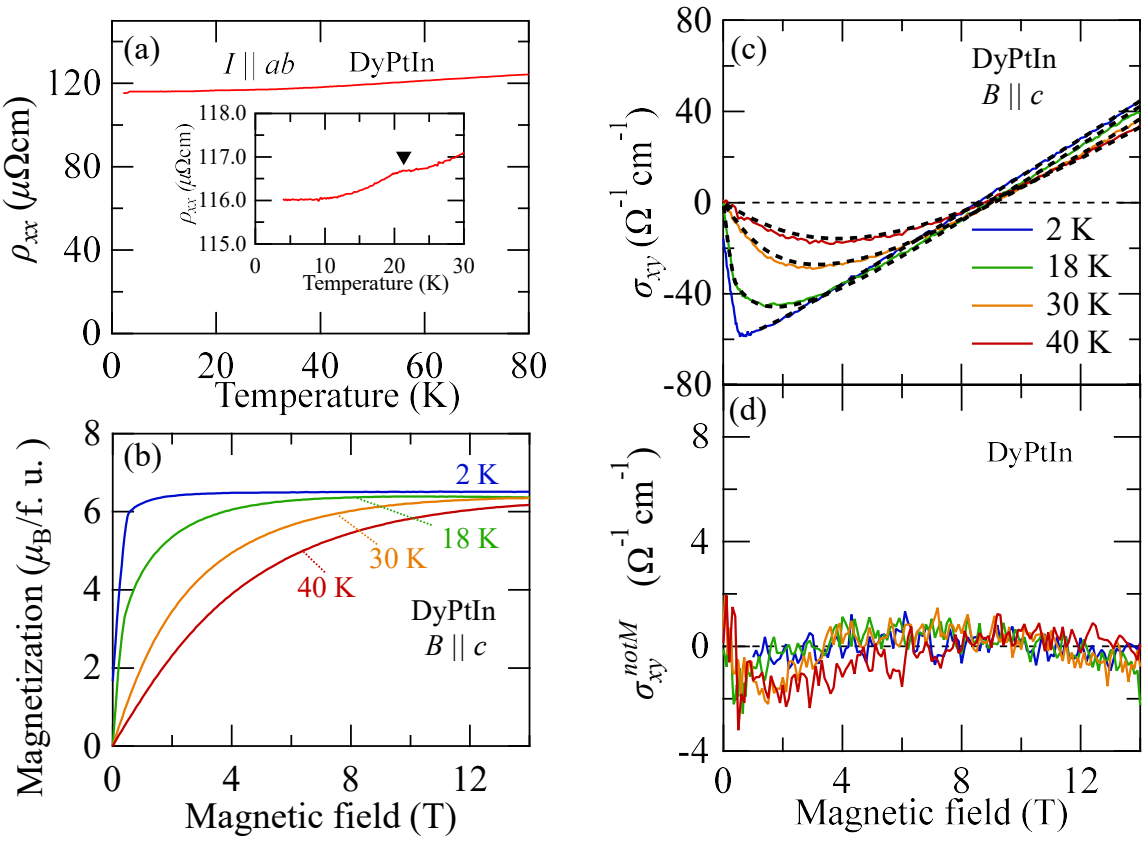

FIG. 7. (a) The temperature dependence of resistivity for DyPtIn under zero magnetic field. (b) Magnetization curve of DyPtIn for $B||c$. (c) The anomalous Hall conductivity proportional to M (σ_{xy}^{M}). The dashed curves denote the sum of the ordinary Hall conductivity and anomalous Hall conductivity proportional to M ($\sigma_{xy}^{O} + \sigma_{xy}^{M}$). (d) Anomalous Hall conductivity not proportional to M (σ_{xy}^{notM}).